From one to two dimensions in quantum spin systems

A. Fledderjohann, K.-H. Mütter, M.-S. Yang and M. Karbach
Physics Department, University of Wuppertal, D-42097 Wuppertal, Germany
(February 1, 2008)

We study the first derivative of the staggered magnetization squared $dm^\dagger(\theta)^2/d\theta$ and the second derivative $d^2e_0(\theta)/d\theta^2$ of the ground state energy per site. The parameter θ controls the anisotropy between horizontal and vertical couplings in a two-dimensional (2D) spin-1/2 antiferromagnetic Heisenberg model. It is shown, that both derivatives diverge at $\theta = 1$, where the anisotropic 2D model reduces to the 1D model.

I. INTRODUCTION

Antiferromagnetism looks different in the 1D and 2D Heisenberg model with nearest-neighbor coupling of spin-1/2 matrices. The zero-temperature staggered magnetization $m^\dagger$ is known to be zero in the 1D and to be nonzero in the 2D model.[1–8] Introducing different strengths for the horizontal and vertical couplings $J_h \equiv J(1+\theta)/2$ and $J_v \equiv J(1-\theta)/2$ the staggered magnetization $m^\dagger(\theta)$ has been studied as a function of the anisotropy parameter θ. It has been found in Ref. 9 $m^\dagger(\theta) \neq 0$ for $0 \leq \theta \leq \theta_0$, where θ_0 is at least $\theta_0 \leq 0.98$.[9] It has been suggested, that $m^\dagger(\theta) \neq 0$ in the whole interval $0 \leq \theta < 1$.

In this paper we study the derivative $dm^\dagger(\theta)^2/d\theta$ and the second derivative $d^2e_0(\theta)/d\theta^2$ of the ground state energy. The transition from one to two dimensions is performed with an interpolating Hamiltonian $\mathbf{H}(\theta)$, defined on system sizes $N = k^2 \pm 1$, $k = 3, 5, ...$ with helical boundary conditions. The θ-evolution of energy eigenvalues and eigenvectors as well as expectation values of hermitian operators is discussed in Sec. II. These general results are applied and numerically evaluated for $dm^\dagger(\theta)^2/d\theta$ and $d^2e_0(\theta)/d\theta^2$ in Sec. III and IV, respectively. Our main result states that both derivatives diverge logarithmically with the system size N at $\theta = 1$.

The origin of these divergences can be traced back to the low energy excitations in the sector with total spin 0 of the 1D antiferromagnetic Heisenberg model. This sector is investigated in Sec. V. In Sec. VI we discuss consequences for the staggered magnetization in the 1D antiferromagnetic Heisenberg model with next to nearest-neighbor couplings.

II. THE INTERPOLATING HAMILTONIAN

Let us start with the 1D Heisenberg Hamiltonian with periodic boundary conditions:

$$\mathbf{H}_1 \equiv \sum_{n=1}^{N} \mathbf{S}_n \cdot \mathbf{S}_{n+1}, \qquad \mathbf{S}_{N+1} = \mathbf{S}_1, \tag{2.1}$$

and $N = k^2 \pm 1$ sites. The interpolating Hamiltonian between one and two dimensions is defined by:

$$\mathbf{H}(\theta) \equiv \frac{1+\theta}{2}\mathbf{H}_1 + \frac{1-\theta}{2}\mathbf{Q}_k\mathbf{H}_1{\mathbf{Q}_k}^\dagger. \tag{2.2}$$

$\mathbf{Q}_k$ represents a permutation operator for the sites on the ring

$$\mathbf{Q}_k S_n^a \mathbf{Q}_k^\dagger = S_{(n-1)k+1}^a, \qquad a = x, y, z, \tag{2.3}$$

which transforms the nearest-neighbor couplings in Hamiltonian (2.1) into couplings between spins separated by $k = \sqrt{N \mp 1}$:

$$\mathbf{Q}_k\mathbf{H}_1\mathbf{Q}_k^\dagger = \sum_{n=1}^{N} \mathbf{S}_n \cdot \mathbf{S}_{n+k}. \tag{2.4}$$

$\mathbf{H}(\theta)$ defines a 2D Hamiltonian with helical boundary conditions,[10,11] as can be seen in Fig. 1 of Ref. 10. The horizontal and vertical couplings have strengths $(1+\theta)/2$ and $(1-\theta)/2$, respectively. The parameter θ controls the interpolation from the 1D Hamiltonian $\mathbf{H}(1) = \mathbf{H}_1$ to the 2D Hamiltonian with equal strength for horizontal and vertical couplings

$$\mathbf{H}_+ \equiv \mathbf{H}(0), \tag{2.5}$$

where

$$\mathbf{H}_\pm \equiv \frac{1}{2}\left(\mathbf{H}_1 \pm \mathbf{Q}_k\mathbf{H}_1\mathbf{Q}_k^\dagger\right). \tag{2.6}$$

The permutation operator $\mathbf{Q}_k$ is essentially a rotation, which transforms horizontal nearest-neighbor couplings into vertical ones. One verifies the equations:

$$\mathbf{Q}_k^2 S_n^a {\mathbf{Q}_k^\dagger}^2 = \begin{cases} S_n^a & : k^2 = N+1 \\ S_{2-n}^a & : k^2 = N-1 \end{cases}, \tag{2.7a}$$

$$\mathbf{Q}_k^4 S_n^a {\mathbf{Q}_k^\dagger}^4 = S_n^a. \tag{2.7b}$$

Therefore, $\mathbf{H}_1$ commutes with $\mathbf{Q}_k^2$, but it does not commute with $\mathbf{Q}_k$:

$$[\mathbf{Q}_k^2, \mathbf{H}_1] = 0, \quad [\mathbf{Q}_k, \mathbf{H}_1] \neq 0. \tag{2.8}$$

The operator $\mathbf{Q}_k$ transforms the interpolating Hamiltonian (2.2) as follows:

$$\mathbf{Q}_k \mathbf{H}(\theta) \mathbf{Q}_k^\dagger = \mathbf{H}(-\theta). \tag{2.9}$$

Note, that $\mathbf{Q}_k$ is a unitary operator

$$\mathbf{Q}_k \mathbf{Q}_k^\dagger = \mathbf{1}, \tag{2.10}$$

and for this reason $\mathbf{H}(\theta)$ and $\mathbf{H}(-\theta)$ are unitary equivalent and possess an identical spectrum of eigenvalues:

$$\mathbf{H}(\theta)|\Psi_n(\theta)\rangle = E_n(\theta)|\Psi_n(\theta)\rangle, \tag{2.11a}$$
$$E_n(\theta) = E_n(-\theta), \tag{2.11b}$$
$$\mathbf{Q}_k|\Psi_n(\theta)\rangle = |\Psi_n(-\theta)\rangle. \tag{2.11c}$$

Let us investigate the θ-evolution of the eigenvalues $E_n(\theta)$ and the eigenvectors $|\Psi_n(\theta)\rangle$. Differentiation of Eq. (2.11a) with respect to θ yields:

$$\frac{dE_n(\theta)}{d\theta}\delta_{mn} = [E_m(\theta) - E_n(\theta)]\langle\Psi_m(\theta)|\Psi_n'(\theta)\rangle + \langle\Psi_m(\theta)|\mathbf{H}_-|\Psi_n(\theta)\rangle. \tag{2.12}$$

For $n = m$ we find, that the θ-evolution of the energy eigenvalues

$$\frac{dE_n(\theta)}{d\theta} = \frac{1}{2\theta}\left[E_n(\theta) - \langle\Psi_n(\theta)|\mathbf{H}(-\theta)|\Psi_n(\theta)\rangle\right], \tag{2.13}$$

is governed by the expectation values of the $\mathbf{Q}_k$-rotated Hamiltonian (2.9). The θ-evolution of the eigenvectors $|\Psi_n(\theta)\rangle$ reads

$$\frac{d}{d\theta}|\Psi_n(\theta)\rangle = -\sum_{m\neq n}\frac{\langle\Psi_m(\theta)|\mathbf{H}_-|\Psi_n(\theta)\rangle}{E_m(\theta) - E_n(\theta)}|\Psi_m(\theta)\rangle, \tag{2.14}$$

which follows from (2.12) for $n \neq m$. This yields for the θ-dependence of matrix elements of hermitian operators $\mathbf{O}(\theta)$:

$$\frac{d}{d\theta}\langle\Psi_m(\theta)|\mathbf{O}(\theta)|\Psi_n(\theta)\rangle = \langle\Psi_m(\theta)|\mathbf{O}'(\theta)|\Psi_n(\theta)\rangle - \sum_{k\neq m}\frac{\langle\Psi_k(\theta)|\mathbf{H}_-|\Psi_m(\theta)\rangle}{E_k(\theta) - E_m(\theta)}\langle\Psi_k(\theta)|\mathbf{O}(\theta)|\Psi_n(\theta)\rangle - \sum_{l\neq n}\frac{\langle\Psi_l(\theta)|\mathbf{H}_-|\Psi_n(\theta)\rangle}{E_l(\theta) - E_n(\theta)}\langle\Psi_l(\theta)|\mathbf{O}(\theta)|\Psi_m(\theta)\rangle. \tag{2.15}$$

In particular we get for the θ-evolution of the expectation values $\langle\Psi_m(\theta)|\mathbf{H}(-\theta)|\Psi_n(\theta)\rangle$, which enter on the right-hand side of (2.13):

$$\frac{d}{d\theta}\langle\Psi_m(\theta)|\mathbf{H}(-\theta)|\Psi_m(\theta)\rangle = \frac{1}{2\theta}\left[\langle\Psi_m(\theta)|\mathbf{H}(-\theta)|\Psi_m(\theta)\rangle - E_m(\theta)\right] + \frac{1}{\theta}\sum_{n\neq m}\frac{|\langle\Psi_n(\theta)|\mathbf{H}(-\theta)|\Psi_m(\theta)\rangle|^2}{E_n(\theta) - E_m(\theta)}. \tag{2.16}$$

It should be noted that the second term on the right-hand side of (2.16) can be expressed in terms of the dynamical structure factor:

$$S_n[\omega; \mathbf{H}(-\theta)] \equiv \sum_{m\neq n}|\langle\Psi_n(\theta)|\mathbf{H}(-\theta)|\Psi_m(\theta)\rangle|^2 \times\delta\big(\omega - [E_m(\theta) - E_n(\theta)]\big), \tag{2.17}$$

associated with the transition operator $\mathbf{H}(-\theta)$.

III. THE FIRST DERIVATIVE OF THE STAGGERED MAGNETIZATION

Equation (2.15) enables us to compute the slope of the staggered magnetization squared:

$$m^\dagger(\theta)^2 \equiv \frac{1}{N}\langle\Psi_0(\theta)|\mathbf{S}^\dagger(\pi)\mathbf{S}(\pi)|\Psi_0(\theta)\rangle, \tag{3.1}$$

where

$$\mathbf{S}(p) \equiv \frac{1}{\sqrt{N}}\sum_{l=1}^{N} e^{ipl}\mathbf{S}_l. \tag{3.2}$$

$m^\dagger(\theta)^2$ is known to be zero for $\theta = 1$ (D=1) and nonzero for $\theta = 0$ (D=2) [$m^\dagger(0) \approx 0.30$ see Refs. 1–8]. It is expected that $m^\dagger(\theta) > 0$ for $0 \leq \theta < 1$. The derivative of the staggered magnetization is of special interest near $\theta = 1$. Using (2.15) and (3.1) it follows:

$$\frac{dm^\dagger(\theta)^2}{d\theta} = -\frac{2}{N}\sum_{m\neq 0}\frac{\langle\Psi_m(\theta)|\mathbf{H}_-|\Psi_0(\theta)\rangle}{\omega_m(\theta)}M_m(\theta,\pi), \tag{3.3}$$

where we have introduced the notation:

$$M_m(\theta, p) \equiv \langle\Psi_m(\theta)|\mathbf{S}(-p)\cdot\mathbf{S}(p)|\Psi_0(\theta)\rangle. \tag{3.4}$$

For the computation of the right-hand side of (3.3) we need the excitation energies $\omega_m(\theta) \equiv E_m(\theta) - E_0(\theta)$, the transition amplitudes $\langle\Psi_m(\theta)|\mathbf{H}_-|\Psi_0(\theta)\rangle$, and $M_m(\theta,\pi)$ in the total spin $S_T = 0$ sector of the interpolating Hamiltonian $\mathbf{H}(\theta)$. Having determined the ground state vector $|\Psi_0(\theta)\rangle$ by means of the Lanczos algorithm, the excitation energies and transition amplitudes can be computed via the recursion method described in Appendix A.

Going back to the definition (2.6) of $\mathbf{H}_-$ and expressing the spin operators $\mathbf{S}_l$ in terms of their Fourier transforms (3.2), we arrive at the following representation of the transition matrix elements:

$$\langle\Psi_m(\theta)|\mathbf{H}_-|\Psi_0(\theta)\rangle = \sum_p\left(e^{-ip} - e^{-ipk}\right)M_m(\theta,p). \tag{3.5}$$

It is important to note that the matrix elements $M_m(\theta,p)$ are constrained by energy conservation for $m \neq 0$:

$$0 = \langle \Psi_m(\theta)|\mathbf{H}(\theta)|\Psi_0(\theta)\rangle,$$
$$= \sum_p \left(\frac{1+\theta}{2} e^{-ip} + \frac{1-\theta}{2} e^{-ipk} \right) M_m(\theta, p). \quad (3.6)$$

The slope of the staggered magnetization (3.3) can now be written as:

$$\frac{dm^\dagger(\theta)^2}{d\theta} = 2 \int_0^{\pi - 2\pi/N} \frac{dp}{\pi} [\cos(pk) - \cos p] \Sigma(\theta, p, \pi, N), \quad (3.7)$$

where we have defined:

$$\Sigma(\theta, p_1, p_2, N) \equiv \sum_{m \neq 0} \frac{M_m(\theta, p_1) M_m(\theta, p_2)}{\omega_m(\theta)}. \quad (3.8)$$

$\Sigma(\theta, p, \pi, N)$ has to obey the sum rule resulting from (3.6):

$$\frac{2}{N} \Sigma(\theta, \pi, \pi, N) = \int_0^{\pi - 2\pi/N} \frac{dp}{\pi} \Sigma(\theta, p, \pi, N) \times [(1+\theta)\cos p + (1-\theta)\cos(pk)]. \quad (3.9)$$

We first discuss the situation for $\theta = 1$ (D=1). As can be seen from Fig. 1, $\Sigma(1, p, \pi, N)$ is negative for $\pi/2 \lesssim p < \pi$, whereas $\Sigma(1, \pi, \pi, N)$ is positive by definition.

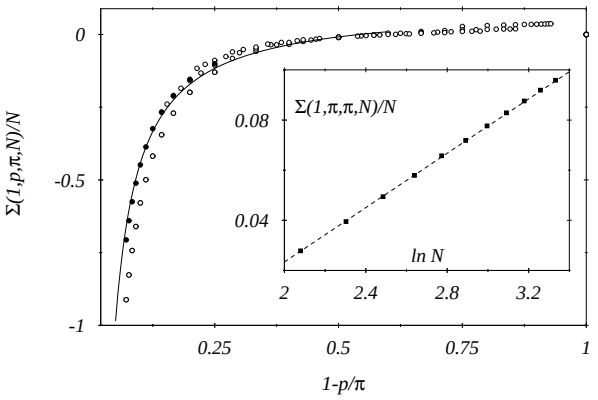

FIG. 1. $\Sigma(1, p, \pi, N)$ with the data of finite systems $N = 8, 10, \ldots, 28$, (○). The solid dots (●) show the forecast inferred from (3.14). The solid line represents the prediction (3.12), whereas the dashed line in the inset represents the corresponding least square fit (3.11) to $\Sigma(1, \pi, \pi, N)$ (3.10).

In the large N limit

$$\frac{1}{N} \Sigma(1, \pi, \pi, N) \stackrel{N \to \infty}{\longrightarrow} A \ln \frac{N}{N_0} \quad (3.10)$$

diverges logarithmically with N, as is shown in the inset of Fig. 1. From a least square fit we estimate:

$$A = 0.0542(5), \qquad N_0 = 1.089(5). \quad (3.11)$$

Owing to the sum rule (3.9), the divergence (3.10) is related to the singularity

$$\Sigma(1, p, \pi, \infty) \stackrel{p \to \pi}{\longrightarrow} \frac{-A}{1 - p/\pi}, \quad (3.12)$$

which we compare in Fig. 1 with finite system results for $\Sigma(1, p, \pi, N)$. Finite-size effects are small for momentum values away from the singularity (3.12). In the combined limit

$$p \to \pi, \quad N \to \infty, \quad z = (1 - p/\pi)N \quad \text{fixed}, \quad (3.13)$$

we try to describe the finite-size effects with a finite-size scaling ansatz:

$$\Sigma(1, p, \pi, N) = \Sigma(1, p, \pi, \infty) G(z), \quad (3.14)$$

which we already used in Ref. 12,13 to analyse singularities of static structure factors. The ansatz allows to predict $\Sigma(1, p, \pi, 2N)$, for $p = \pi(1 - 4/N)$ and $2N = 32, 36, \ldots, 56$. This prediction is shown in Fig. 1 by the dots (●). These points yield a smooth extrapolation of the numerical results for $z = 4$, $N = 16, 18, \ldots, 28$ which are already close to the predicted behavior (3.12), represented by the solid curve in Fig. 1. The importance of the singularity (3.12) is obvious, it yields the leading contribution to the derivative of $m^\dagger(\theta)^2$ in the limit $N \to \infty$:

$$\left. \frac{dm^\dagger(\theta)^2}{d\theta} \right|_{\theta=1} \stackrel{N \to \infty}{\longrightarrow} 2A \int_{2\pi/N}^{\pi} \frac{dp}{p} [\cos(pk) - \cos p], \stackrel{N \to \infty}{\longrightarrow} -A \ln N. \quad (3.15)$$

We would like to stress, that the singularity (3.15) becomes visible only by following the arguments presented above. In particular, the sum rule (3.9) and the divergence (3.10) of the susceptibility $\Sigma(1, \pi, \pi, N)$ in the 1D case are crucial for the derivation of (3.12).

One might wonder whether the singularity of $dm^\dagger(\theta)^2/d\theta$ at $\theta = 1$ can be seen as well in the θ-dependence. For this purpose we have evaluated (3.3) on systems of size $N = k^2 \mp 1$, $k = 3, 5$. The results for $dm^\dagger(\theta)^2/d\theta$ as a function of θ are shown in Fig. 2.

For all systems the first derivative $dm^\dagger(\theta)^2/d\theta$ is negative and decreases in the range $0 < \theta < \theta_m(N)$, passes a minimum at $\theta_m(N)$ and then increases again, by passing a turning point $\theta_t(N)$ near $\theta = 1$. How to reconcile this behavior with our bias for the thermodynamic limit of $dm^\dagger(\theta)^2/d\theta$? We expect a decrease for $0 < \theta < 1$, a singularity

$$\frac{dm^\dagger(\theta)^2}{d\theta} \stackrel{\theta \to 1^-}{\longrightarrow} -\infty, \quad (3.16)$$

if we approach the 1D limit from the left and

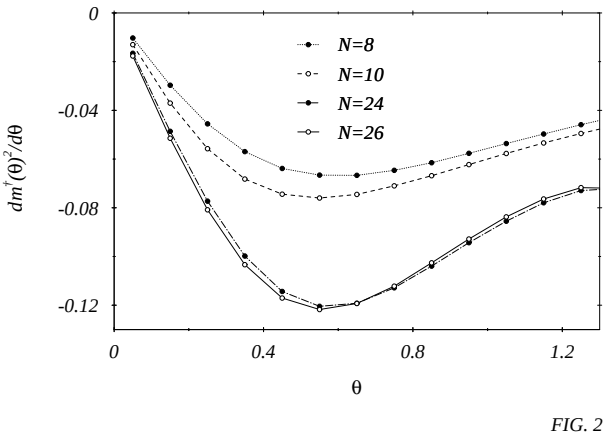

FIG. 2. The derivative $dm^\dagger(\theta)^2/d\theta$ for finite systems, evaluated via Eq. (3.3).

$$\frac{dm^\dagger(\theta)^2}{d\theta} = 0 \tag{3.17}$$

for $\theta > 1$. For $\theta > 1$ the horizontal and vertical couplings in (2.2) are antiferromagnetic and ferromagnetic, respectively. In this situation, the staggered magnetization is supposed to vanish.

If the scenario (3.16) and (3.17) is correct, there should be a sharp discontinuity in $dm^\dagger(\theta)^2/d\theta$ when we pass the transition point $\theta = 1$. For the finite systems – presented in Fig. 2 – this sharp discontinuity is washed out. The transition region starts already at the minimum $\theta_m(N) < 1$ and extends far beyond the transition point $\theta = 1$. Therefore, we expect that for increasing system size the minimum position $\theta_m(N)$ converges to the transition point $\theta = 1$:

$$\theta_m(N) \stackrel{N\to\infty}{\longrightarrow} 1, \tag{3.18}$$

whereas the minimum value diverges:

$$\left.\frac{dm^\dagger(\theta)^2}{d\theta}\right|_{\theta=\theta_m(N)} \stackrel{\theta\to 1^-}{\longrightarrow} -\infty. \tag{3.19}$$

Comparing in Fig. 2 the results for $N = 8, 10, 24, 26$, we see already that the slope of $dm^\dagger(\theta)^2/d\theta$ becomes steeper for $\theta > \theta_m(N)$. This feature could be interpreted as a signature for the emergence of the discontinuity (3.16) and (3.17) in the thermodynamic limit. However, it certainly requires larger systems to observe this process.

IV. THE SECOND DERIVATIVE OF THE GROUND STATE ENERGY

According to (2.13) the first derivative of the ground state energy per site $e_0(\theta)$ at $\theta = 1$,

$$\left.\frac{de_0(\theta)}{d\theta}\right|_{\theta=1} = \frac{1}{2}e_0(1), \tag{4.1}$$

is given by the ground state energy $e_0(1) = -(\ln 2 - 1/4)$ itself.[14] Here we have used the fact that the ground state expectation value[15,16]

$$\frac{1}{N}\langle\Psi_0|\mathbf{H}(-1)|\Psi_0\rangle = \langle\Psi_0|\mathbf{S}_0\mathbf{S}_k|\Psi_0\rangle \stackrel{k\to\infty}{\longrightarrow} -a\frac{\sqrt{\ln k}}{k},$$

vanishes in the limit $k = \sqrt{N \mp 1} \to \infty$. Combining (2.13) and (2.16), we find for the second derivative:

$$\frac{d^2e_0(\theta)}{d\theta^2} = -\frac{2}{N}\sum_{m\neq 0}\frac{|\langle\Psi_m(\theta)|\mathbf{H}_-|\Psi_0(\theta)\rangle|^2}{\omega_m(\theta)}. \tag{4.2}$$

The Fourier decomposition (3.5) of the transition matrix elements $\langle\Psi_m(\theta)|\mathbf{H}_-|\Psi_0(\theta)\rangle$ leads to the representation:

$$\begin{aligned}\frac{d^2e_0(\theta)}{d\theta^2} = &-4\int_0^{\pi-2\pi/N}\frac{dp}{\pi}[\cos p - \cos(pk)]^2\Sigma(\theta,p,p,N)\\ &-4N\int_0^{\pi-2\pi/N}\int_0^{p-2\pi/N}\frac{dp}{\pi}\frac{dp'}{\pi}\\ &\times[\cos p - \cos(pk)][\cos p' - \cos(p'k)]\Sigma(\theta,p,p',N).\end{aligned} \tag{4.3}$$

$\Sigma(\theta, p_1, p_2, N)$ is defined in (3.8) and numerical results for $\theta = 1$ and $N = 24$ are given in Table I. Note, that $\Sigma(\theta = 1, p_1, p_2, N) < 0$ for $\pi/2 \lesssim p_2 < p_1 < \pi$, whereas $\Sigma(\theta = 1, p, p, N) > 0$ by definition.

TABLE I. $\Sigma(\theta, p_1, p_2, N)$ [Eq. (3.8)] for $N = 24$ and $p_1, p_2 = 2\pi l/N$, $l = 4, 5, \ldots, 12$.

l	4	5	6	7	8	9	10	11	12
4	**0.005**	-0.001	-0.001	-0.002	-0.006	0.000	0.002	0.003	0.002
5	-0.001	**0.007**	-0.002	-0.006	-0.001	0.001	0.001	0.001	-0.001
6	-0.001	-0.002	**0.006**	-0.001	0.000	0.001	0.001	0.000	-0.005
7	-0.002	-0.006	-0.001	**0.018**	-0.000	-0.000	-0.001	-0.002	-0.011
8	-0.006	-0.001	0.000	-0.000	**0.030**	-0.002	-0.003	-0.005	-0.022
9	0.000	0.001	0.001	-0.000	-0.002	**0.050**	-0.007	-0.012	-0.045
10	0.002	0.001	0.001	-0.000	-0.003	-0.007	**0.096**	-0.029	-0.106
11	0.003	0.001	0.000	-0.002	-0.005	-0.012	-0.029	**0.231**	-0.371
12	0.002	-0.001	-0.005	-0.011	-0.022	-0.045	-0.106	-0.371	**1.051**

$\Sigma(\theta, p, p', N)$ and $\Sigma(\theta, p, \pi, N)$ are related via the energy conservation relation (3.6):

$$\begin{aligned}&[(1+\theta)\cos p + (1-\theta)\cos(pk)]\Sigma(\theta,p,p,N)\\ &\quad -\Sigma(\theta,p,\pi,N) = \Delta(\theta,p,N),\end{aligned} \tag{4.4}$$

where

$$\begin{aligned}\Delta(\theta,p,N) \equiv -\frac{N}{2\pi}&\left(\int_0^{p-2\pi/N}dp' + \int_{p+2\pi/N}^{\pi-2\pi/N}dp'\right)\\ &\times[(1+\theta)\cos p' + (1-\theta)\cos(p'k)]\Sigma(\theta,p,p',N).\end{aligned} \tag{4.5}$$

The sum rule (4.4) for $\theta = 1$ yields important constraints for $p \to \pi$, where $\Sigma(1, p, \pi, \infty)$ develops the pole

(3.12) depicted in Fig. 1. This pole has to be compensated by a corresponding singularity in:

$$\Sigma(1,p,p,\infty) \stackrel{p\to\pi}{\longrightarrow} \frac{B}{1-p/\pi}, \tag{4.6}$$

which is indeed observable in the numerical data shown in Fig. 3. The finite-size effects can be treated again with a finite-size scaling ansatz of the type (3.14). The open symbols (○) represent the prediction of this ansatz. The solid curve is a pole fit of the type (4.6) with:

$$B = 0.053(10). \tag{4.7}$$

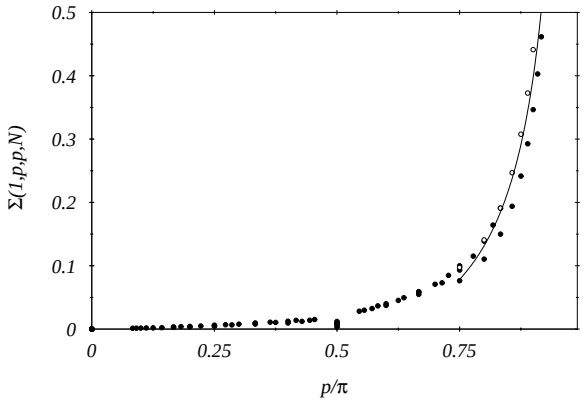

FIG. 3

FIG. 3. $\Sigma(1,p,p,N)$ for finite systems $N = 8, 10, \ldots, 28$ (•) and the predicted pole (4.6) in conjunction with (4.7) for $\Sigma(1,p,p,\infty)$ (solid line).

The pole for $p \to \pi$ appears as well on the left-hand side (4.4) of the sum rule:

$$\Delta(\theta = 1, p, N) \stackrel{p\to\pi}{\longrightarrow} \frac{A-2B}{1-p/\pi}. \tag{4.8}$$

The right-hand side of (4.5) tells us, how $\Sigma(\theta=1,p,p',N)$ behaves for $p, p' \to \pi$ in order to generate the pole term (4.8) on the right-hand side of (4.4):

$$N \ln N \Sigma(1,p,p',N) \stackrel{p\neq p'\to\pi}{\longrightarrow} \frac{A-2B}{(1-p/\pi)(1-p'/\pi)}. \tag{4.9}$$

Insertion of the leading singularities (4.6) and (4.9) into the right-hand side of (4.3) yields

$$\left.\frac{d^2 e_0(\theta)}{d\theta}\right|_{\theta=1} \stackrel{N\to\infty}{\longrightarrow} -\frac{1}{2}(A+2B)\ln N. \tag{4.10}$$

In Fig. 4 we present the θ-dependence of the second derivative $d^2 e_0(\theta)/d\theta^2$ on finite systems $N = 8, 10, 24, 26$, as it follows from (4.2). There is no signature in the finite system results, which give a hint to the singularity (4.10). A comparison of (4.2) with a numerical differentiation of the ground state energy yields excellent agreement.

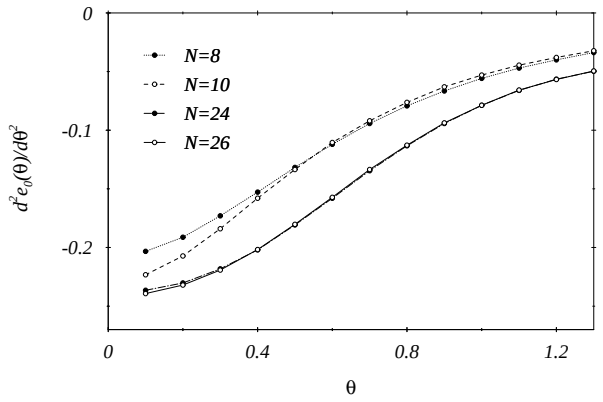

FIG. 4

FIG. 4. The second derivative of the ground state energy $e_0(\theta)$ versus θ as it follows from Eq. (4.2).

V. LOW ENERGY EXCITATIONS IN THE SPIN 0 SECTOR OF THE 1D ANTIFERROMAGNETIC HEISENBERG MODEL

The singular behavior of the first derivative of the staggered magnetization and of the second derivative of the ground state energy per site can be traced back to the divergence (3.10) of the quantity:

$$\Sigma(\theta = 1, \pi, \pi, N) = \int_{\omega_1(N)}^{\infty} \frac{d\omega}{\omega} S(\omega, \pi, N), \tag{5.1}$$

which again can be viewed as the susceptibility of the dynamic structure factor

$$S(\omega, p, N) \equiv \sum_{n\neq 0} M_n(1,p)^2 \delta(\omega - \omega_n). \tag{5.2}$$

The operators $\mathbf{S}(-p)\cdot\mathbf{S}(p)$, which enter in the definition (3.4), only allow for transitions with $\Delta S = 0$ and $\Delta p = 0$. The gap $\omega_1(N)$ in the sector with quantum numbers of the ground state vanishes in the thermodynamic limit

$$N\omega_1 \stackrel{N\to\infty}{\longrightarrow} \Omega_1 = 25.15(5), \tag{5.3}$$

as is shown in Fig. 5.

The divergence (3.10) of the susceptibility (5.1) demands for an infrared singularity in the dynamic structure factor at $p = \pi$

$$S(\omega, \pi, N) \stackrel{\omega\to 0}{\longrightarrow} A\frac{\Omega_1}{\omega}\ln\frac{1}{\omega}, \tag{5.4}$$

which is visible in the numerical data for the scaled transition probabilities (3.4) of Fig. 6, in spite of the rather large finite-size effects.

Insertion of (5.4) into (5.1) leads to (3.10).

In Fig. 7 we present the p-dependence of the excitation energies $\omega_n = E_n - E_0$ for $N = 24$ together

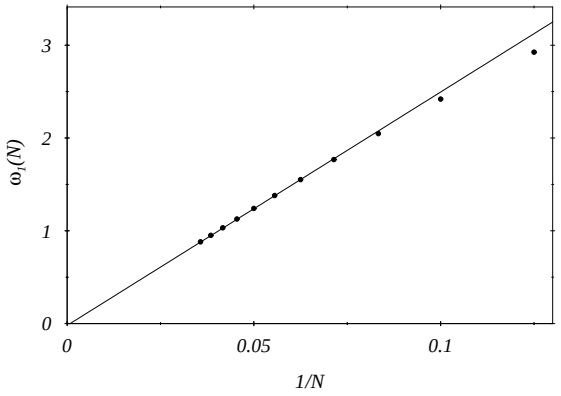

FIG. 5

FIG. 5. The excitation gap $\omega_1(N)$ for $N = 8, 10, \ldots, 28$. The solid line represents the fit (5.3).

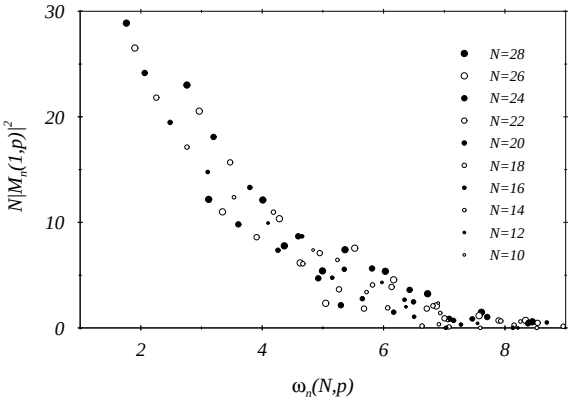

FIG. 6

FIG. 6. The scaled transition probabilities (3.4) for finite systems ($N = 10, ..., 28$) vs. the excitation energy.

with the associated relative spectral weights in percentage terms. Highest spectral weights occur at excitation energies $\omega_{max}(p)$. This curve is rather well approximated by

$$\omega_{max}(p) = \pi \sin p. \tag{5.5}$$

The dashed curve is the dispersion relation for the lowest excitations in the $S_T = 0$-sector in the thermodynamic limit:

$$\omega_L(p) = \frac{\pi}{2} \sin p, \tag{5.6}$$

as it was calculated in Ref. 17. On our finite system we find nonvanishing excitation also below $\omega_L(p)$, they will not survive in the thermodynamic limit.

Finally let us discuss the connected correlators:

$$C(p,N) \equiv \langle \Psi_0(1)|\mathbf{S}(p)^2\mathbf{S}(p)^2|\Psi_0(1)\rangle$$

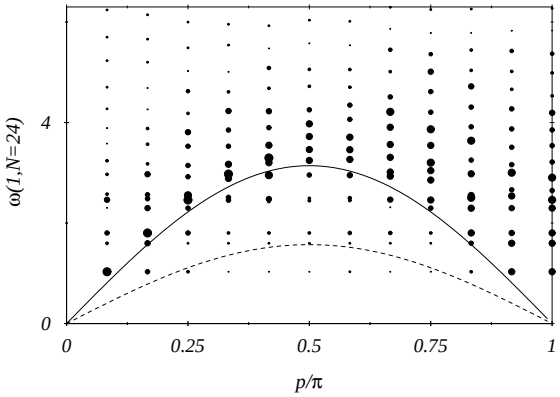

FIG. 7

FIG. 7. The excitation spectrum for $\theta = 1$ and $N = 24$. The size of the dots is proportional to the relative spectral weights of associated transition matrix elements $M_n(1,p)^2$.

$$-\langle \Psi_0(1)|\mathbf{S}(p)^2|\Psi_0(1)\rangle^2,$$
$$= \int_{\omega_1(N)}^{\infty} d\omega S(\omega, p, N), \tag{5.7}$$

which follow by integrating up the dynamic structure factor (5.4). The infrared singularity (5.4) induces a divergence in $C(\pi, N)$ for $N \to \infty$:

$$C(\pi, N) \stackrel{N\to\infty}{\longrightarrow} \frac{A}{2}\Omega_1 (\ln N)^2. \tag{5.8}$$

This behavior is clearly seen in Fig. 8. The slope of the numerical data in the inset of Fig. 8 is 0.525(8), which deviates from the prediction (3.11) and (5.3):

$$\frac{A}{2}\Omega_1 = 0.682(5). \tag{5.9}$$

by about -23%.

The p-dependence of the static structure factor (5.7) is given in Fig. 8. One observes a singularity at $p = \pi$. Finite-size effects are small, away from the singularity. Near the singularity they can be described with a finite-size scaling ansatz in the fashion (3.14) we used for $\Sigma_1(\theta = 1, \pi, p_1, N)$ in Sec. III.

In summary: The N-dependence of the susceptibility $\Sigma(\theta = 1, \pi, \pi, N)$ and of the connected correlators $C(\pi, N)$ as well as the p-dependence of $\Sigma(\theta = 1, p, p, N)$ and $C(p, N)$ support the existence of the infrared singularity (5.4) in the dynamic structure factor (5.2).

VI. THE 1D ANTIFERROMAGNETIC HEISENBERG MODEL WITH NEXT TO NEAREST-NEIGHBOR COUPLINGS

The approach developed in Secs. II - IV is applicable to all Hamiltonians $\mathbf{H}(\vartheta)$ which depend on a parameter

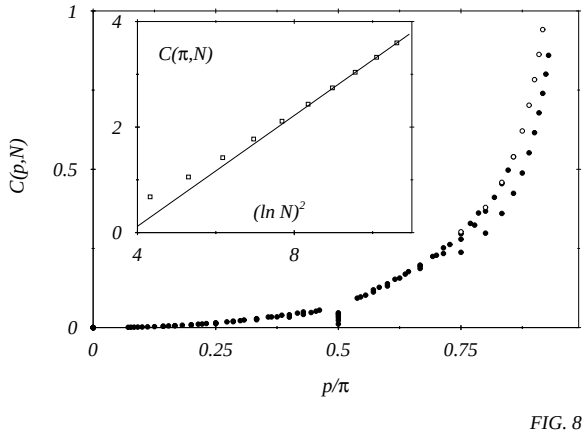

FIG. 8

FIG. 8. The connected correlators (5.7) for $N = 8, \ldots, 28$ are shown as solid symbols (•), whereas the prediction of a finite-size scaling ansatz is marked by open symbols (○). The inset represents the singular behavior of $C(\pi, N)$ together with the corresponding fit (5.8).

ϑ and reduce to the 1D Heisenberg Hamiltonian for the specific value $\vartheta = 1$. As a further example we consider the Hamiltonian

$$\mathbf{H}(\vartheta) = \mathbf{H}_1 + (\vartheta - 1)\mathbf{H}_2, \tag{6.1}$$

with next to nearest-neighbor couplings

$$\mathbf{H}_2 \equiv \sum_{n=1}^{N} \mathbf{S}_n \cdot \mathbf{S}_{n+2}. \tag{6.2}$$

These couplings strengthen the antiferromagnetism for $\vartheta < 1$, but frustrate the system for $\vartheta > 1$. Therefore, the question arises, what happens here with the staggered magnetization for $\vartheta \leq 1$. Repeating the arguments which lead to (3.7), yields for the first derivative of the staggered magnetization squared:

$$\left.\frac{dm^\dagger(\vartheta)^2}{d\vartheta}\right|_{\vartheta=1} = -2\int_0^{\pi(1-2/N)} \frac{dp}{\pi}[\cos(2p) + \cos p] \times \Sigma(\vartheta = 1, p, \pi, N). \tag{6.3}$$

Again $\Sigma(\vartheta = 1, p, \pi, N)$ is given by (3.8) in terms of the excitation energies $\omega_m(\vartheta = 1) = E_m(\vartheta = 1) - E_0(\vartheta = 1)$ and transition probabilities $M_m(1, p)$ of the 1D nearest-neighbor model with Hamiltonian $\mathbf{H}(\vartheta = 1)$. However, insertion of the pole term contribution (3.12) leads here to a *finite* contribution for $dm^\dagger(\vartheta)^2/d\vartheta|_{\vartheta=1}$ in the thermodynamic limit. It is worthwhile to note how the range of the spin-spin couplings – over 2 lattice spacings in (6.1) and over $k = \sqrt{N \mp 1}$ lattice spacings in (2.2) – enters via the Fourier factors $\cos(2p)$ and $\cos(kp)$ in the formulas (6.3) and (3.7) for $dm^\dagger(\vartheta)^2/d\vartheta|_{\vartheta=1}$, respectively. These Fourier factors generate the different behavior of $dm^\dagger(\vartheta)^2/d\vartheta|_{\vartheta=1}$ in the two cases (6.1) and (2.2).

VII. SUMMARY AND CONCLUSIONS

It is convenient to study the transition from one to two dimensions by means of an interpolating Hamiltonian $\mathbf{H}(\theta)$ [cf.(2.2)] with a parameter θ, which controls the anisotropy between the horizontal and vertical nearest-neighbor couplings. The quantity of interest is the staggered magnetization $m^\dagger(\theta)$, which on one hand is supposed to be nonzero for the anisotropic 2D model $(0 \leq \theta < 1)$ and which on the other hand is known to be zero in the 1D limit $\theta = 1$. In this paper we have studied the first derivative $dm^\dagger(\theta)^2/d\theta$. It can be expressed in terms of excitation energies $\omega_n = E_n - E_0$ and transition matrix elements $\langle\Psi_m|\mathbf{S}(-p)\mathbf{S}(p)|\Psi_0\rangle$ associated with the operator $\mathbf{S}(-p) \cdot \mathbf{S}(p)$.

In other words, the θ-evolution of the staggered magnetization (3.7) is determined by the dynamics in the sector with total spin $S_T = 0$ and momentum transfer $\Delta p = 0$. Energy conservation sum rules (3.6) yield important constraints on the transition matrix elements $\langle\Psi_m(\theta)|\mathbf{S}(-p)\mathbf{S}(p)|\Psi_0(\theta)\rangle$. They turned out to be very helpful in our numerical analysis of the low-energy excitations at $\theta = 1$:

1. The dynamic structure factor (5.2) has an infrared singularity (5.4) at $p = \pi$. For $0 < p < \pi$, there is a dispersion relation $\omega = \omega_L(p)$ (5.6) for the lowest excitations (with $\Delta S = 0$ and $\Delta p = 0$) in the thermodynamic limit. On finite systems, we find excitations below $\omega_L(p)$.

2. The existence of the infrared singularity is supported by the divergences, which can be clearly seen in the N dependence of the connected correlators $C(\pi, N)$ (5.8) and the susceptibility $\Sigma(1, \pi, \pi, N)$ (3.10) and in the p-dependence of $C(p, N)$ and $\Sigma(1, p, p, N)$ for $p \to \pi$.

3. Owing to the energy conservation sum rule (3.9), the divergence in the susceptibility induces a pole (3.12) in $\Sigma(1, p, \pi)$. This pole term fixes the leading large-N behavior (3.15) of the first derivative in the staggered magnetization squared at $\theta = 1$.

We have considered in this paper the transition from one to two dimensions in the spin 1/2-antiferromagnetic Heisenberg model only. However, the general formulas (3.3) and sum rule (3.6), which describe the θ-evolution, hold as well in the spin-1 case, where the 1D model $(\theta = 1)$ develops the celebrated *Haldane gap*.[18,19] The existence of this gap already tell us, that there is no infrared singularity of the type (5.1). Therefore, we do not expect a divergence (3.15) in $dm^\dagger(\theta)^2/d\theta|_{\theta=1}$ in the spin 1 case

APPENDIX: RECURSION METHOD

The recursion method is designed to approximately determine the excitation energies and matrix elements of

transition operators, the dynamics of which are to be studied. Neglecting indices like momentum p and chain length N let us consider

$$f_A(\omega) = \sum_n |\langle n|A|0\rangle|^2 \delta[\omega - (E_n - E_0)], \tag{A1}$$

with $|0\rangle$, $|n\rangle$ being the ground state and the excited states of the system defined by the Hamiltonian H. E_0 and E_n are the corresponding energies. (e.g. A might be chosen as $A = S_j(p,N), \quad j = 1,2,3$). The Laplace transform of $f_A(\omega)$ reads

$$f_A(\tau) = \sum_n e^{-\omega_n \tau} |\langle n|A|0\rangle|^2, \tag{A2}$$

$$= \langle 0|A^+ e^{-(\mathbf{H}-E_0)\tau} A|0\rangle = \langle f_0|f(\tau)\rangle, \tag{A3}$$

with $|f_0\rangle = A|0\rangle$ and $|f(\tau)\rangle$ fulfilling

$$\frac{\partial}{\partial \tau}|f(\tau)\rangle = -\bar{\mathbf{H}}|f(\tau)\rangle, \qquad (\bar{\mathbf{H}} = \mathbf{H} - E_0). \tag{A4}$$

Now, a Gram-Schmidt construction is used (see also Ref. 20) to form an orthogonal set of states $\{|f_k\rangle\}$, namely

$$|f_{k+1}\rangle = \bar{\mathbf{H}}|f_k\rangle - a_k|f_k\rangle - b_k^2|f_{k-1}\rangle \tag{A5}$$

$$a_k = \frac{\langle f_k|\bar{\mathbf{H}}|f_k\rangle}{\langle f_k|f_k\rangle}, \quad k = 0,1,2,..,L-1, \tag{A6a}$$

$$b_0^2 \equiv 0, \tag{A6b}$$

$$b_k^2 = \frac{\langle f_k|f_k\rangle}{\langle f_{k-1}|f_{k-1}\rangle}, \quad k = 1,2,..,L-1, \tag{A6c}$$

and $|f(\tau)\rangle$ is expressed as

$$|f(\tau)\rangle = \sum_{k=0}^{L-1} \mathbf{D}_k(\tau)|f_k\rangle. \tag{A7}$$

L denotes the dimension of the Hilbert space, i.e. the number of states $|n\rangle$ leading to nonzero matrix elements $\langle n|A|0\rangle$. The differential equation (A4) leads to

$$\sum_k \dot{\mathbf{D}}_k(\tau)|f_k\rangle = -\sum_k \mathbf{D}_k(\tau)\left(|f_{k+1}\rangle + a_k|f_k\rangle + b_k^2|f_{k-1}\rangle\right) \tag{A8}$$

or in matrix notation $\dot{\vec{\mathbf{D}}} = -\mathbf{M}\vec{\mathbf{D}}$ with $\mathbf{M}$ being a tridiagonal $L\times L$-matrix with eigenvalues ω_n and eigenvectors $\vec{e}_n$. The eigensolutions $v_k(\tau)$ of the set of linear differential equations read $v_k(\tau) = v_k^0 e^{-\omega_k \tau}$ leading to

$$\mathbf{D}_k(\tau) = \sum_n (\vec{e}_n)_k v_n^0 e^{-\omega_n \tau}. \tag{A9}$$

Here, the v_k^0 are given by the initial condition $\vec{\mathbf{D}}(\tau = 0) = (1,0,0,...,0)^T$ yielding for $f_A(\tau)$

$$f_A(\tau) = \mathbf{D}_0(\tau)\langle f_0|f_0\rangle = \sum_n e^{-\omega_n \tau} v_n^0 (\vec{e}_n)_0 \langle f_0|f_0\rangle, \tag{A10}$$

i.e. $|\langle n|A|0\rangle|^2 = v_n^0(\vec{e}_n)_0\langle f_0|f_0\rangle$. It should be noted that the eigenvalues of $\mathbf{M}$ are real, however, its non non-symmetric structure does not require the $\vec{e}_n$ to be orthogonal. The approximation in our scheme sets in in the fact that the numerical treatment does not allow for generating the whole set of L orthogonal states. The number of iterations in (A5) is reduced to $\tilde{L}$, the matrix $\mathbf{M}$ truncated to $\tilde{L}\times\tilde{L}$ and the evaluation given above is performed on this reduced set of states. Details and checks for this method are given in Refs. 21,22.

In the present paper the recursion method has been extended [see e.g. Eq. (3.3)] to treat matrix elements of type

$$\langle g|f(\tau)\rangle = \langle g|e^{-\tau\bar{\mathbf{H}}}|f_0\rangle, \tag{A11}$$

with $|f_0\rangle = \mathbf{A}|0\rangle$, $|g\rangle = \mathbf{B}|0\rangle$, $\mathbf{A}$ and $\mathbf{B}$ acting on the same space. Using the series representation of $|f(\tau)\rangle$ we obtain

$$\langle 0|\mathbf{B}^+|n\rangle\langle n|\mathbf{A}|0\rangle = \sum_k v_n^0(\vec{e}_n)_k\langle g|f_k\rangle, \tag{A12}$$

which contains the transition probabilities $|\langle n|\mathbf{A}|0\rangle|^2$ for the choice $\mathbf{B} = \mathbf{A}$.

[1] T. Kennedy, E. Lieb, and B. Shastry, J. Stat. Phys. **53**, 1019 (1988).
[2] S. Tang and J. Hirsch, Phys. Rev. B **39**, 4548 (1989).
[3] R. Singh, Phys. Rev. B **39**, 9760 (1989).
[4] S. Liang, Phys. Rev. B **42**, 6555 (1990).
[5] Z. Weihong, J. Oitmaa, and C. Hamer, Phys. Rev. B **43**, 8321 (1991).
[6] T. Barnes, Int. J. Mod. Phys. C **2**, 659 (1991).
[7] H. Schulz and T. Ziman, Europhys. Lett. **18**, 355 (1992).
[8] C. Canali and M. Wallin, Phys. Rev. B **48**, 3264 (1993).
[9] I. Affleck, M. Gelfand, and R. Singh, J. Phys. A: Math. Gen. **27**, 7313 (1994).
[10] O. Haan, J.-U. Klaetke, and K.-H. Mütter, Phys. Rev. B **46**, 5723 (1992).
[11] M.-S. Yang and K.-H. Mütter, Z. Phys. B **??**, ?? (1997).
[12] M. Karbach and K.-H. Mütter, Z. Phys. B **90**, 83 (1993).
[13] M. Karbach, K.-H. Mütter, and M. Schmidt, Phys. Rev. B **50**, 9281 (1994).
[14] L. Hulthén, Arkiv Mat. Astron. Fysik **26A 11**, 1 (1938).
[15] R. R. P. Singh, M. E. Fisher, and R. Shankar, Phys. Rev. B **39**, 2562 (1989).
[16] I. Affleck, D. Gepner, H. J. Schulz, and T. Ziman, J. Phys. A: Math. Gen. **22**, (1989).
[17] J. D. Johnson and B. M. McCoy, Phys. Rev. A **6**, 1613 (1972).
[18] F. D. M. Haldane, Phys. Lett. **93A**, 464 (1983).

[19] I. Affleck, J. Phys.: Condens. Matter **1**, 3047 (1989).
[20] V. S. Viswanath and G. Müller, *The Recursion Method*, *LNP m23* (Springer-Verlag, Berlin-Heidelberg, 1994).
[21] A. Fledderjohann, M. Karbach, K.-H. Mütter, and P. Wielath, J. Phys.: Condens. Matter **7**, 8993 (1995).
[22] A. Fledderjohann *et al.*, Phys. Rev. B **54**, 7168 (1996).